Check for updates

Studying the influence of axial substituents on hyperfluorescence in organic light-emitting diodes using boron subphthalocyanines as fluorescent emitters†

Owen A. Melville,[a] Rachel Zigelstein, [iD][a]
Trevor Plint[a] and Timothy P. Bender [iD] *[abcd]

Boron subphthalocyanines (BsubPcs) are a class of macrocycles that are often stable and straightforward to synthesize. Their optical properties such as high extinction coefficient and strong fluorescence have led to their incorporation into optoelectronic devices including OLEDs. However, the best demonstrated OLEDs using BsubPc emitters were unable to convert triplet excitons generated through applied bias into light. To address this, we fabricated OLEDs incorporating an assistant dopant into the emissive layer, 2-phenyl-4′-carbazole-9H-thioxanthen-9-one-10,10-dioxide (TXO-PhCz), capable of thermally converting triplet excitons into singlets, which are then transferred to the BsubPc emitter, a process referred to as hyperfluorescence. We also varied the axial substituent attached to the BsubPc core to determine its effect on the resulting performance. We found that the use of the TADF assistant dopant increased current efficiency up to 200% while maintaining more than 90% emission from the BsubPc in most cases. The best BsubPcs had short alkoxy axial groups, achieving an average current efficiency of 1.34 cd A^{-1} across a luminance range of up to ~10^3 cd m^{-2} using *tert*-butoxy BsubPc. These devices are the most efficient, and pure color OLEDs demonstrated using BsubPcs as the primary emitter at reasonable luminance outputs. These findings highlight the promise of BsubPc emitters in high-performance OLEDs when paired with a TADF assistant dopant, offering a viable route to efficient and color-pure devices.

Design, System, Application

Boron subphthalocyanines (BsubPcs) are unique organic macrocyclic compounds that are being developed and studied as active materials in organic electronic devices, such as within organic light emitting diodes (OLEDs). The basic chemistry of axial and/or peripheral substitutions enables variation in the functionalization of BsubPc derivatives and influences the physical properties of the BsubPc macrocycles. The past study did focus on variations of the axial substituent groups to see if any physical properties and other relevant properties were to be taken into consideration for further organic electronic applications. As seen in the past study, there was no major change in the absorption spectral peaks based on the axial substituents, no major change of the HOMO–LUMO energy levels *via* electrochemical characterization and no differentiation in stability. Chemistry wise, we studied the array of eighteen axially substituted BsubPcs, which started from the Br–BsubPc precursor, with the B–Br bond having axial substituents, and therefore was achieved with good yield. This outcome of the past study supported the investigation of incorporation of an array of BsubPc axial substituents in OLEDs. Therefore, to see if light emissions from the BsubPcs within the OLEDs emite appropriately, we then used 2-phenyl-4′-carbazole-9H-thioxanthen-9-one-10,10-dioxide as a host, which upon electrical excitation was thermally converted to the triplet-state, transferring energy to the BsubPcs. This led to light emissions from BsubPcs and showed the pure colour characteristics of the light emissions. Given our array of BsubPcs, some were found to have better emission properties in OLEDs, as outlined in our study report.

[a] Department of Chemical Engineering & Applied Chemistry, University of Toronto, 200 College Street, Toronto, Ontario, M5S 3E5, Canada.
E-mail: tim.bender@utoronto.ca; Tel: +416 978 6140
[b] Department of Chemistry, University of Toronto, 80 St. George Street, Toronto, Ontario, M5S 3H6, Canada
[c] Department of Mechanical & Industrial Engineering, University of Toronto, 5

King's College Road, Toronto, Ontario, M5S 3G8, Canada
[d] Department of Materials Science and Engineering, University of Toronto, 184 College Street, Toronto, Ontario, M5S 3E4, Canada
† Electronic supplementary information (ESI) available: Method for estimating layer thickness; tables of data; figures of data. See DOI: https://doi.org/10.1039/d5me00019j

This journal is © The Royal Society of Chemistry and IChemE 2025

Mol. Syst. Des. Eng., 2025, **10**, 957–969 | 957

Introduction

Conjugated carbon-based molecules are a broad class of materials with promising commercial applications in optoelectronic devices such as organic photovoltaics (OPVs) and organic light-emitting diodes (OLEDs). While OLEDs have seen widespread success in displays, particularly in smartphones and TVs, high-performance red-orange emitters often rely on iridium complexes that are costly and unsustainable due to iridium's rarity. Organic molecules with more sustainable syntheses offer an attractive alternative but require careful optimization of both efficiency and color purity.

Boron subphthalocyanines (BsubPcs, Fig. 1a) are stable, synthetically accessible macrocycles with several optoelectronic advantages. The high extinction coefficient of BsubPcs makes them promising light-absorbing materials, with 3% efficient solar cells demonstrated as early as 2007.[1] More recently,

BsubPcs have been used to increase the stability of OPVs as electron donors,[2] as electron acceptors[3] and as interfacial stabilizers in perovskite solar cells.[4]

The photoluminescence quantum yield (PLQY) reported was as high as 85%,[5] and the narrow emission of BsubPcs makes them good candidates for narrow orange-red emitters in OLEDs. In 2007, Torres *et al.* reported the first example of solution-processed OLEDs using solubilized BsubPcs as emitters.[6] Despite lacking a host in the emissive layer as is typical in more modern OLED architectures, the current efficiency of these devices reached a maximum of 0.1 cd A^{-1} (cd A^{-1} = candelas per ampere). Vacuum-deposited OLEDs using phthalimido boron subphthalocyanines without a host demonstrated a current efficiency of up to 0.02 cd A^{-1}.[7] Using a similar device architecture, pentafluorophenoxy boron subphthalocyanine (F$_5$-BsubPc, **8**) devices demonstrated current efficiencies of up to 0.03 cd A^{-1}.[8] Helander *et al.*
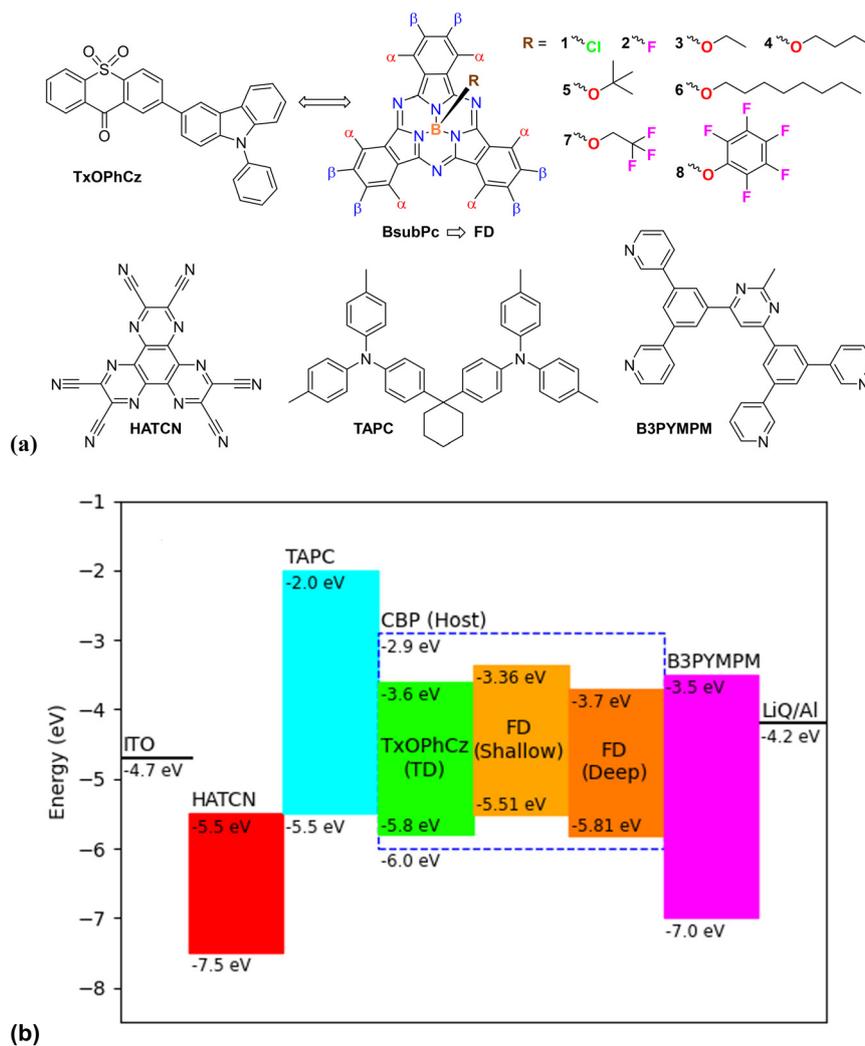
Fig. 1 a) Diagram of an axially substituted (**R**) boron phthalocyanine (BsubPc) and the list of BsubPcs utilized in this study (**1–8**). α and β are also called peripheral substitutions of the BsubPcs and for the list utilized in this study, α and β = H. The list of other materials are given as well. b) Energy level diagram for the OLEDs used in this study. The light and dark orange energy bars for the fluorescent dopant (FD) represent the maximum and minimum HOMO and LUMO energy levels in materials **1–8**, which were estimated using a BsubPc-specific correlation.[20] The TXO-PhCz TADF assistant dopant was not present in baseline devices. Energy levels for the other organic layers were referenced from Ossila.

958 | *Mol. Syst. Des. Eng.*, 2025, **10**, 957–969

This journal is © The Royal Society of Chemistry and IChemE 2025

improved on this performance by incorporating a host material, 4,4′-bis(carbazol-9-yl)biphenyl (CBP), demonstrating a current efficiency of up to 1.5 cd A^{-1} at low luminances.[9] In 2018, Plint et al. achieved a maximum current efficiency of 1.3 cd A^{-1} for chloro boron subphthalocyanine (Cl-BsubPc, **1**) OLEDs.[10] In 2023, Farac et al. demonstrated solution-processed OLEDs using partially peripherally fluorinated BsubPcs with a stable current efficiency of up to 0.34 cd A^{-1}.[11]

Despite these promising characteristics, OLEDs using BsubPcs as the primary fluorescent dopants (FDs) have demonstrated issues with the overall performance and color purity. The devices reported by Helander et al. using 20% BsubPc in CBP for the emissive layer demonstrated a maximum current efficiency of 1.5 cd A^{-1} at an ultra-low luminance around 0.1 cd m^{-2} (cd m^{-2} = candelas per square meter), which decayed to about 0.15 cd A^{-1} at higher luminances between 10^2 and 10^3 cd m^{-2} that are more relevant to display and lighting applications.[9] When the researchers decreased the BsubPc concentration to 1% to reduce concentration quenching, this drop in performance with luminance was not as pronounced, retaining a current efficiency of 0.4 cd A^{-1} at a luminance of 10^3 cd m^{-2}. This improvement came with a cost, as the OLED's emission became contaminated with blue light from the host or transport layers which comprised around 43% of the spectra by intensity. To capitalize on this color impurity, Plint et al. focused on white-light emission, as their 1.3 cd A^{-1} OLEDs only demonstrated a maximum of 66% light intensity from the BsubPc fluorescent emitter.[10] Thus, OLEDs using BsubPcs as the primary emitter for narrow orange emission with a current efficiency above 1 cd A^{-1} in relevant luminance ranges have yet to be demonstrated.

One strategy to improve the emission properties of OLEDs is to use thermally activated delayed fluorescence (TADF).[12] During electrically induced excitation, triplet states are generated at a ratio of 3 : 1 compared to singlet states. However, light emission is typically restricted to radiative decay from the singlet state due to the conservation of spin, limiting the maximum conversion of excitons to light to 25% for fluorescent emitters. In some molecules, the triplet energy is close enough to the singlet energy for thermally activated reverse intersystem crossing (RISC), unlocking the potential for a four-fold increase in OLED emission efficiency. One example of a TADF-based emitter is 2-phenyl-4′-carbazole-9H-thioxanthen-9-one-10,10-dioxide (TXO-PhCz), a broad green emitter incorporated into OLEDs with a reported current efficiency of up to 76 cd A^{-1}.[13] The emission spectra of such TADF-based OLEDs tend to be broad, which can negatively affect the color purity in display applications.[14]

Although narrow-band fluorescent emitters like BsubPcs do not demonstrate the narrow singlet-triplet gap required for TADF, incorporating a TADF-capable assistant dopant (TD) into the OLED emissive layer can increase their emission efficiency. The TD molecules can transfer energy to fluorescent dopants (FDs) via Forster resonance energy transfer (FRET). This process of RISC followed by FRET is a

process referred to as hyperfluorescence.[15] Adachi et al. demonstrated hyperfluorescence for blue, green, yellow and red emission in 2014.[16] The orange-red emitter DBP, combined with a green-emitting TD, tri-PXZ-TRZ, resulted in OLEDs with a current efficiency between 20 and 25 cd A^{-1}. Without the TD, device performance deteriorated significantly, demonstrating the power of the hyperfluorescence architecture. Despite this success, residual emission from the TD emitter could be clearly observed in the output spectra, lowering the color purity for DBP, already a broad emitter. Since then, red-orange hyperfluorescence has been demonstrated with several different FD/TD pairings.[17–19]

For example, Kwon et al. combined a novel BODIPY-based red emitter, 4tBuMB, with two TADF assistants, 4Cz-TPN and 4Cz-IPN.[18] The resulting OLEDs demonstrated a current efficiency between 24 and 26 cd A^{-1} with emission from the TD completely suppressed at 0.7 wt% 4tBuMB paired with 4Cz-TPN. Thus, the devices demonstrated exceptional performance and color purity, with an emission FWHM of only 44 nm. Compared to 4Cz-TPN, 4Cz-IPN demonstrated lower color purity and performance when combined with the fluorescent 4tBuMB in hyperfluorescent OLEDs. The researchers attributed these differences to two major factors. First, the stronger spectral overlap between 4Cz-TPN and 4tBuMB should increase the rate of FRET between the two molecules, enhancing emission from the FD. Second, the relatively deep LUMO level of 4Cz-TPN should suppress electron trapping in the emissive layer compared to 4Cz-IPN.

Indeed, the energy levels (HOMO and LUMO) of the transport layers, the host, TD and FD all impact the performance of an OLED.[14] Ideally, electrons and holes are driven from the electrodes into the emissive layer where they become trapped, with fluorescence recombination on the FD being the main path to recombination. In BsubPcs, the axial and peripheral groups (Fig. 1) can be substituted, changing the HOMO and LUMO energies along with other properties such as PLQY and absorption and emission spectra.[20–24] Thus, the choice of substituents are likely to impact OLED performance, including the color point, compatibility with specific TADF assistant molecules, current efficiency and color purity. Other factors that impact OLED performance include the material choice[25] and thickness[26] of non-emissive layers, the composition and thickness of the emissive layer,[27] and the device surface area.[28]

In this study, we report the first hyperfluorescent OLEDs using BsubPcs as the fluorescent dopants and TXO-PhCz as the TADF assistant dopant. We restrict the peripheral substitution (α/β positions, Fig. 1) to hydrogen and systematically vary the axial substituent to evaluate its effect on device performance. We examine the effects of this axial group, device composition and input voltage on the current efficiency and color purity. Many of the resulting OLEDs outperform previously reported BsubPc-based devices in both metrics. Our best devices demonstrated a current efficiency between 1.7 and 2.5 cd A^{-1} and an emission intensity from
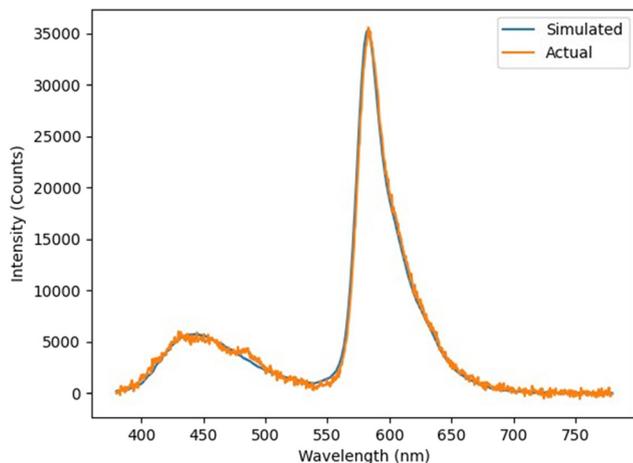
Fig. 2 Sample spectral output of the FD = Cl-BsubPc (**1**) baseline OLEDs, showing the measured emission and the deconvoluted emission.

the FD between 90 and 95% at 250 cd m^{-2}. In the spirit of open science, we also publish our raw data, analysis code, and visualization tools for community use.

Results and discussion

1. Baseline OLEDs

1a. Stack & Design. To investigate the effect of changing the BsubPc axial group substituents on OLED performance, we selected an array of BsubPcs (**1–8**), listed and shown in Fig. 1a. These materials were previously synthesized and characterized for absorbance and fluorescence spectra, relative photoemission quantum yield (PLQY) and HOMO/LUMO energies (using DFT

and cyclic voltammetry).[20] They have similar quantum yields and emission wavelengths and vary primarily in their HOMO/LUMO energy levels. Prior to evaluating the benefit of introducing a TADF-assistant dopant (TD), we first produced host:dopant OLEDs without a TD. The band diagram for these devices is shown in Fig. 1b. The TAPC hole transport layer (HTL) should block electrons due to a shallow LUMO level, while the B3PYMPM electron transport layer (ETL) should block holes due to a deep HOMO level.[14] The energy levels of the FD are encased within that of the CBP host, with the LUMO approximately matching that of the ETL and the HOMO matching that of the HTL. This energetic alignment is favorable for exciton trapping on the FD emitter, which is beneficial for OLED emission.

1b. Variation in the composition. Since the substrate platform in the evaporator does not rotate, and the materials are evaporated from point sources, each of the 20 OLEDs or 'pixels' have distinct compositions for all components, including the ratio of CBP to FD in the emissive layer. To account for these variations, we prepared tooling films for each material, and then measured their thickness variations using a profilometer at 20 distinct points. Using a spatial mapping fitting these data to an *a* plane (detailed in ESI† Section S1), layer thicknesses were estimated for each pixel. For example, a 30 nm nominal TAPC thickness varies from 26.1 nm to 33.6 nm in a set of *n* = 20 devices. Since the variations are assigned to fit planes specific to the material and evaporator source, often these changes are correlated or anti-correlated with each other, making it difficult to infer the specific cause of changes in performance. As shown in ESI† Table S2, the average current efficiency was not highly correlated to any thickness change for FD-only devices, with

Table 1 Summary output data from non-hyperfluorescent OLEDs with different FD emitters/FD materials. All reported values are the median from a set of 20 pixels

Emissive layer composition	FD HOMO energy[e] (eV)	FD LUMO energy[e] (eV)	Turnon voltage[a] (V)	Current efficiency[b] (cd A^{-1})	Emission intensity from[c,d] FD (%)	Emission wavelength[c] (nm)	FWHM[c] (nm)
1: Cl-BsubPc	−5.75	−3.61	3.8	0.26 (0.30)	82.04	583.5	32.5
1: Cl-BsubPc + 20% TxOPhCz			3.2	0.71 (1.03)	91.19	584.5	34.5
2: F-BsubPc	−5.65	−3.50	3.5	0.34 (0.41)	85.31	580.5	32
2: F-BsubPc + 20% TxOPhCz			3.3	0.98 (1.23)	90.87	581	33
3: EtO-BsubPc	−5.54	−3.40	3.5	0.33 (0.36)	88.5	577.5	29.5
3: EtO-BsubPc + 20% TxOPhCz			3.1	0.96 (1.61)	95.46	579	34
4: BuO-BsubPc	−5.55	−3.41	3.5	0.55 (0.65)	94.13	577.5	30.5
4: BuO-BsubPc + 20% TxOPhCz			3.1	1.23 (1.82)	92.29	578	31.5
5: *t*BuO-BsubPc	−5.51	−3.36	3.6	0.48 (0.57)	97.77	578	29
5: *t*BuO-BsubPc + 20% TxOPhCz			3.1	1.34 (1.99)	91.71	577.5	29.5
6: OcO-BsubPc	−5.53	−3.38	3.5	0.45 (0.68)	93.76	577.5	31
6: OcO-BsubPc + 20% TxOPhCz			3.1	1.88 (2.44)	54.57	577	33.5
7: F$_3$EtO-BsubPc	−5.71	−3.57	3.7	0.3 (0.33)	90.75	579.5	31
7: F$_3$EtO-BsubPc + 20% TxOPhCz			3.3	0.61 (0.70)	92.08	580	32
8: F$_5$-BsubPc	−5.75	−3.63	4	0.36 (0.41)	84.96	580.5	30.5
8: F$_5$-BsubPc + 20% TxOPhCz			3.3	0.56 (0.83)	88.01	581	33
20% TxOPhCz	N/A	N/A	3	2.52 (3.31)	0.00	531.5	82.25

[a] Turn-on voltage defined as the voltage that exceeds a luminance of 2 cd m^{-2}. [b] Current efficiency shows the average (maximum) value above the turn-on voltage. [c] All values were captured at an output luminance of 250 cd m^{-2}. [d] Defined as the percentage (by intensity) of the FD emission (Fig. 2). [e] Values previously published and obtained using the BsubPc-specific calibration from density functional theory modeling.[20]

960 | *Mol. Syst. Des. Eng.*, 2025, **10**, 957–969

This journal is © The Royal Society of Chemistry and IChemE 2025

a maximum average absolute correlation coefficient $|r|$ of 0.51. This suggests that the overall OLED performance for these devices was insensitive to the layer thickness variations caused by the evaporator's geometry.

1c. Spectral variation. Fig. 2 shows the typical spectral output for a baseline OLED without the TADF assistant. The large narrow peak on the right is the emission from the BsubPc FD, while the broad blue emission on the left, with a peak around 450 nm, matches none of the materials in the device. This spectrum matches that of the exciplex emission of the electron transport material (B3PYMPM) and its isomers mixed with CBP.[29,30] Notably, a blue emission profile

attributed to exciplex formation was also observed by Helander *et al.* with a 1% BsubPc composition in the emissive layer, but with a peak closer to 425 nm.[9] To determine the relative color purity as listed in Table 1, we separated the emission components in the spectra into blue and orange components by intensity. This quality was found for each device and input voltage. The emission spectra for each OLED material, including the variation from the composition, are shown in Fig. 3.

The relative contribution of blue to orange light changes systematically for almost all samples as a function of position, with the average absolute correlation coefficient
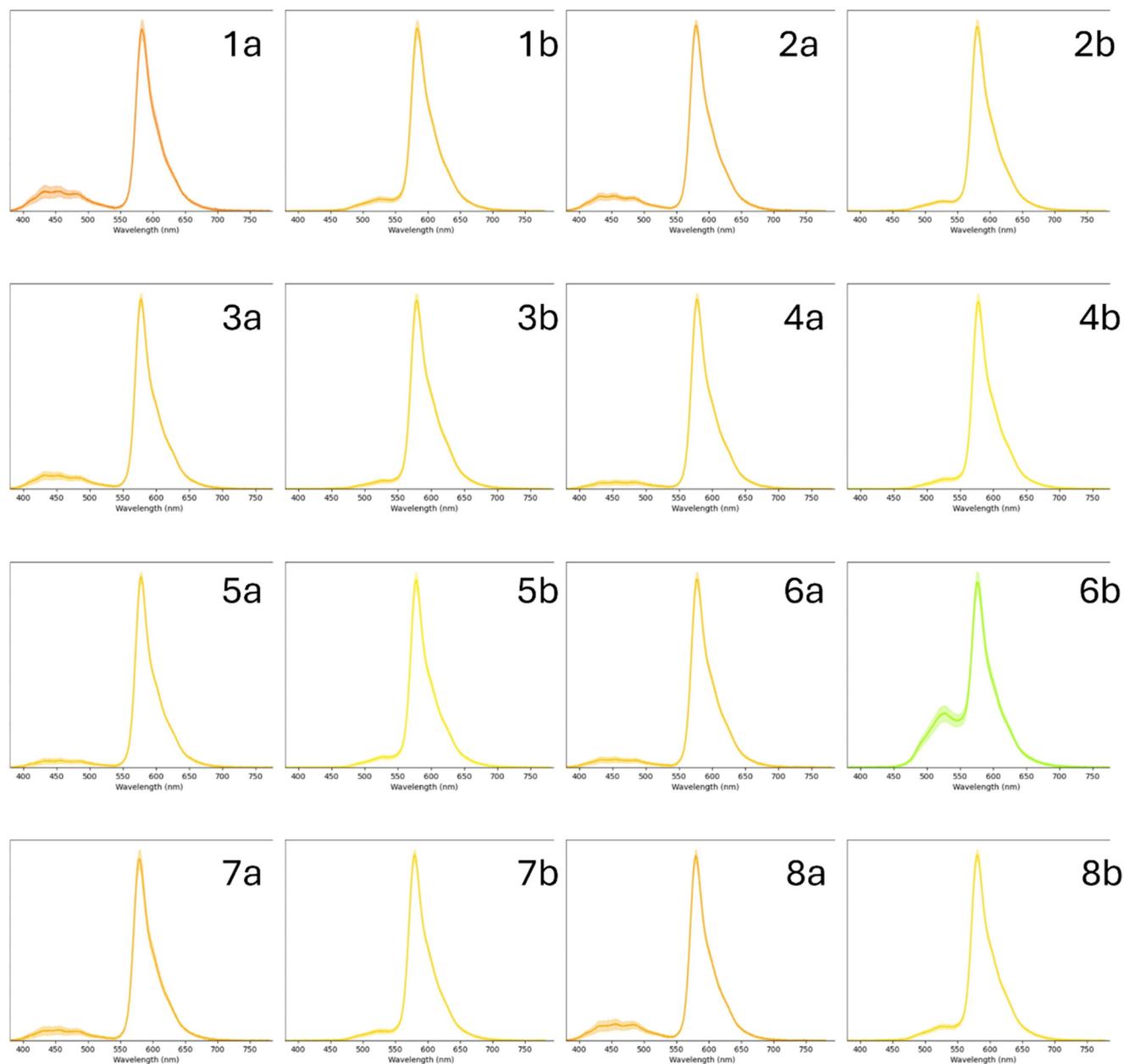

Fig. 3 Emission spectra of all OLEDs with fluorescent emitters **1–8** taken at L = 250 cd m^{-2}. All spectra marked as (a) are devices without TxO-PhCz and those marked with (b) have 20% nominal TxO-PhCz. The blurring of the spectra denotes the standard deviation of the spectra due to compositional variation.

This journal is © The Royal Society of Chemistry and IChemE 2025

Mol. Syst. Des. Eng., 2025, **10**, 957–969 | 961

shown by the material in Table S3† as high as $|r| = 0.97$. This strongly suggests that at least one material thickness affects the color purity. Helander *et al.* observed an increase in blue light with a lower BsubPc concentration, explained by a
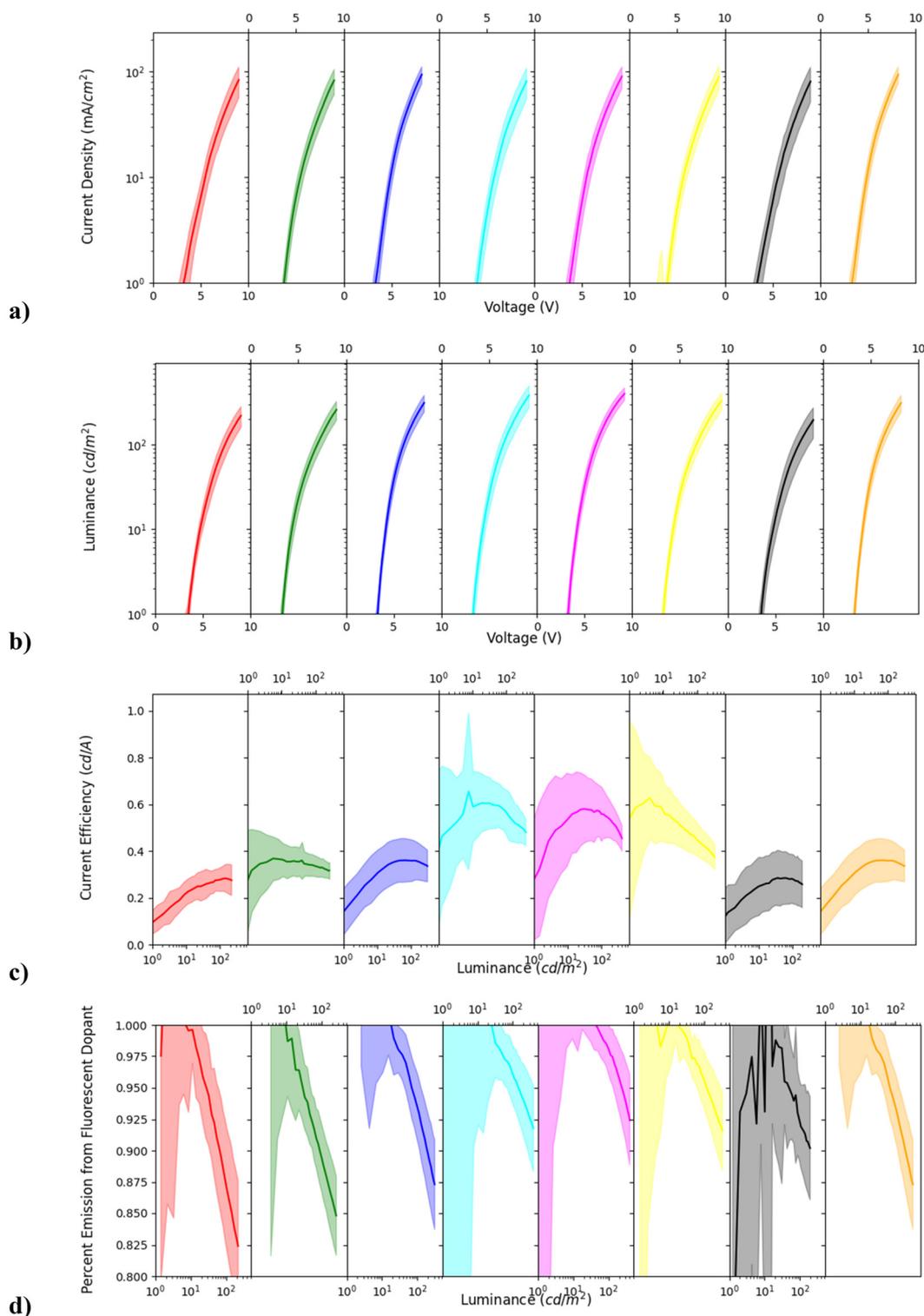
Fig. 4 Average optoelectronic properties for each set of baseline OLEDs from BsubPc material **1** (left) to material **8** (right) (**1**–**8** being the axial substituents, Fig. 1). The properties shown are (a) current density as a function of applied voltage, (b) measured luminance output as a function of applied voltage, (c) current efficiency as a function of luminance output and (d) estimated contribution from the fluorescent dopant as a function of luminance output, estimated by separating the blue and orange emission components as illustrated in Fig. 7. The shaded area represents the standard deviation within the set of compositionally variant devices.

962 | *Mol. Syst. Des. Eng.*, 2025, **10**, 957–969

This journal is © The Royal Society of Chemistry and IChemE 2025

decrease in the charge trapping efficiency.[9] This is consistent with the strong positive correlation (average $r = 0.88$) found between orange light contribution and the FD (BsubPc) concentration in this study.

1d. Effect of the applied voltage. As shown in Fig. 4, the overall performance of the non-hyperfluorescent OLEDs as well as their spectral composition varied as a function applied bias. Above the threshold voltage, luminance steadily increases along with the current (Fig. 4b). The current efficiency for most devices tends to increase and then stabilize at higher luminance outputs (Fig. 4c). Due to this variation, it is possible to report both a maximum and average current efficiency to better capture device performance. The relative spectral contribution of orange light from the FD also increases with luminance output, indicating a decreased efficiency of charge trapping in the emissive layer (Fig. 4d).

1e. Effect of the axial group. The composite results for each set of non-hyperfluorescent OLEDs are shown in Table 1. The shape of the emission spectra varied little, with the peak emission wavelength ranging from 577.5 to 583.5 nm and full-width at half-maximum (FWHM) ranging from 29 to 32.5 nm. As demonstrated in Fig. 4a, the current drawn from each device did not change significantly. As shown in Fig. 4b, luminance output varied slightly by the material, with the turn-on voltage ranging from 3.5 to 4 V. This resulted in an average current efficiency that ranged between 0.26 (for **1**) and 0.55 cd A^{-1} (for **4**). Three possible factors that could affect the data are PLQY, molecular weight, and HOMO/LUMO energy values.

The PLQY for these BsubPcs, reported in a previous study,[20] might impact the fluorescence conversion of excitons to light in the solid state. Despite this, no correlation was observed between the solution-measured PLQY of the BsubPcs and their performance in baseline OLEDs. Cl-BsubPc

(**1**), which demonstrated the highest PLQY, had the lowest overall current efficiency of 0.26 cd A^{-1}. Many of the other materials had similar PLQY values, therefore there is no linear trend (Table 1), and BuO-BsubPc had the highest current efficiency 0.55 cd A^{-1}.

Since the emissive layer composition was controlled at a ratio of 99 : 1 in terms of the rate, *i.e.* 0.99 Å s^{-1} CBP and 0.01 Å s^{-1} FD, the molecular weight of the FD (ESI,† Table S6) should impact its molar concentration. Because of fluorescence quenching, variations in FD concentrations might impact the OLED performance. Despite this possibility, Fig. S2 in the ESI† suggests no clear correlation between the molecular weight and any output parameter.

The HOMO and LUMO energy levels for each material, reported in a previous study and listed in Table 1 were estimated using a BsubPc-specific calibration of values calculated using density functional theory modeling.[20] As seen in Fig. 5, performance tended to improve for BsubPcs with more shallow LUMO levels, with a decreasing turn-on voltage and increasing current efficiency. This could be due to the better alignment with the HOMO of the FD with the reported HOMO of the HTL (−5.5 eV) and/or the LUMO of the FD with the reported LUMO of the ETL (−3.5 eV). This alignment can improve charge trapping and recombination in host : dopant OLEDs.[14] The materials with the best performance as fluorescent dopants in all categories were axial substituents **4–6**, with medium length alkoxy chains (butoxy, *tert*-butoxy and octoxy) as the axial groups.

2. Hyperfluorescent OLEDs

2a. Stack and design. To create hyperfluorescent OLEDs with enhanced BsubPc emission, we incorporated a TADF assistant molecule (TD), TXO-PhCz, into the emissive layer at a 20% rate percent. TXO-PhCz was chosen due to the high
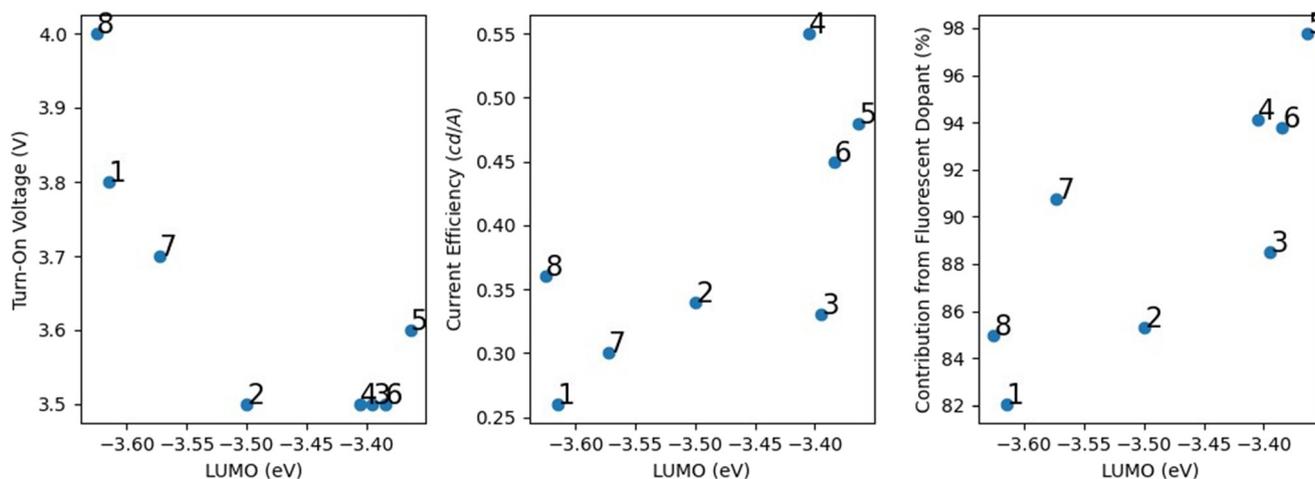
Fig. 5 Effect of the LUMO energy on the turn-on voltage[a], current efficiency[b] and fluorescent dopant contribution[c,d] for baseline OLEDs. [a]Turn-on voltage is defined as the voltage that exceeds a luminance of 2 cd m^{-2}. [b]Current efficiency shows the average value above the turn-on voltage, taken as a median across devices in the same set. [c]All values were captured at an output luminance of 250 cd m^{-2}. [d]Defined as the percentage (by intensity) of the FD emission. FD materials **1–8** BsubPc (Fig. 1) numbers here.

spectral overlap between its emission profile and the absorption profile of BsubPcs **1–8**, which is required for FRET between the two molecules. Fig. 6 shows the spectral overlap between the emission of TxO-PhCz in toluene[13] with the absorption of Cl-BsubPc (**1**) in toluene, which is similar to the absorption profiles of the other BsubPcs.[20] Fig. 1b shows a diagram of the energy levels for the hyperfluorescent devices. An alternative TD, tri-PXZ-TRZ, demonstrated excellent performance (>9 cd A^{-1} current efficiency above turn-on) in the absence of BsubPcs, but did not enhance their emission.

2b. Compositional variation. The composition of the hyperfluorescent devices also varied spatially with the additional element, TXOPhCz, ranging between 16% and 24% of the emissive layer by rate. Table S3† lists the correlations between the overall current efficiency of the devices and the individual layer thicknesses. In general, no clear correlation between any component and current efficiency was observed consistently. This means that the overall electron–photon conversion is somewhat invariant to the composition in these devices, or that any trends are masked by measurement errors or opposing effects. However, for materials **3–5** and **8**, there appeared to be a negative correlation between the FD concentration and overall performance, which could be explained by fluorescence quenching, the quenching being if BsubPcs are close together at the nano level.

2c. Spectral variation. Fig. 7 shows the typical spectral output for an OLED with the TADF assistant, TXO-PhCz (~525 nm). Overall, the FWHM and emission wavelength of these spectra did not vary significantly from the baselines. However, the "blue" contribution from the ETL or host was no longer clear and was replaced by green emission from TXO-PhCz. Due to this emission and that of the FD overlap, the individual components were separated using the same method as the baseline OLEDs. The sum of the deconvoluted components produced simulated fits with good agreement
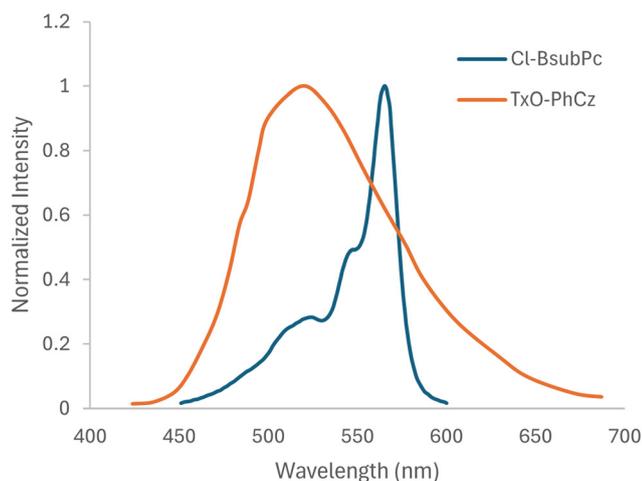
with the measured data (average $R^2 > 0.98$ at $L = 250$ cd m^{-2}), but in some cases there was some deviation. This could indicate a change in the shape of the TXO-PhCz spectra and could lead to some uncertainty in the quantification of relative spectral contribution. Despite this, clear trends were observed between the layer thicknesses within a set of OLEDs and the relative spectral contribution (Fig. S4†), like the baseline OLEDs. The most likely candidate for causing this change is the BsubPc-FD. In the absence of sufficient BsubPc emission sites, some TxOPhCz singlets will recombine, emitting green light. Increasing the density of BsubPc dopants should decrease this likelihood, increasing the relative amount of orange FD emission. Emission spectra of all hyperfluorescent OLEDs, including the spectral variation, are shown in Fig. 3.

2d. Effect of the applied voltage. Fig. 8 summarizes the optoelectronic properties of the OLEDs doped with 20% TXO-PhCz as a function of applied voltage. Compared to the baseline devices, these draw a similar amount of current, but have a lower turn-on voltage and emit higher luminance consistently, leading to a much-improved current efficiency. This efficiency shows a clear roll-off effect,[31] leading to substantial differences between the average and maximum values (Table 1). In addition, the relative contribution from the FD decreased at higher luminance, much like that with the baseline devices. This effect was mitigated by the increased concentration of the FD, suggesting that it is due to the reduced availability of fluorescence sites leading to emission directly from the TD. Overall, this increase in performance, observed for all the BsubPcs, is indicative of successful energy transfer from the TD to the FD. This is consistent with the process of hyperfluorescence.[15]

2e. Effect of the axial group. The effect of the axial group of the BsubPcs on hyperfluorescent OLED properties is shown in Table 1. The turn-on voltage of all devices varied
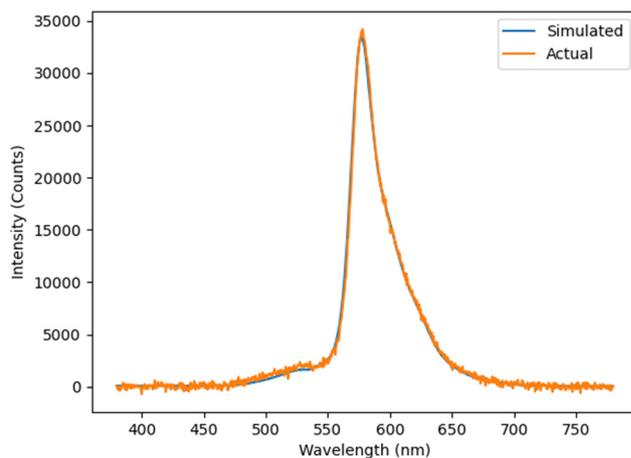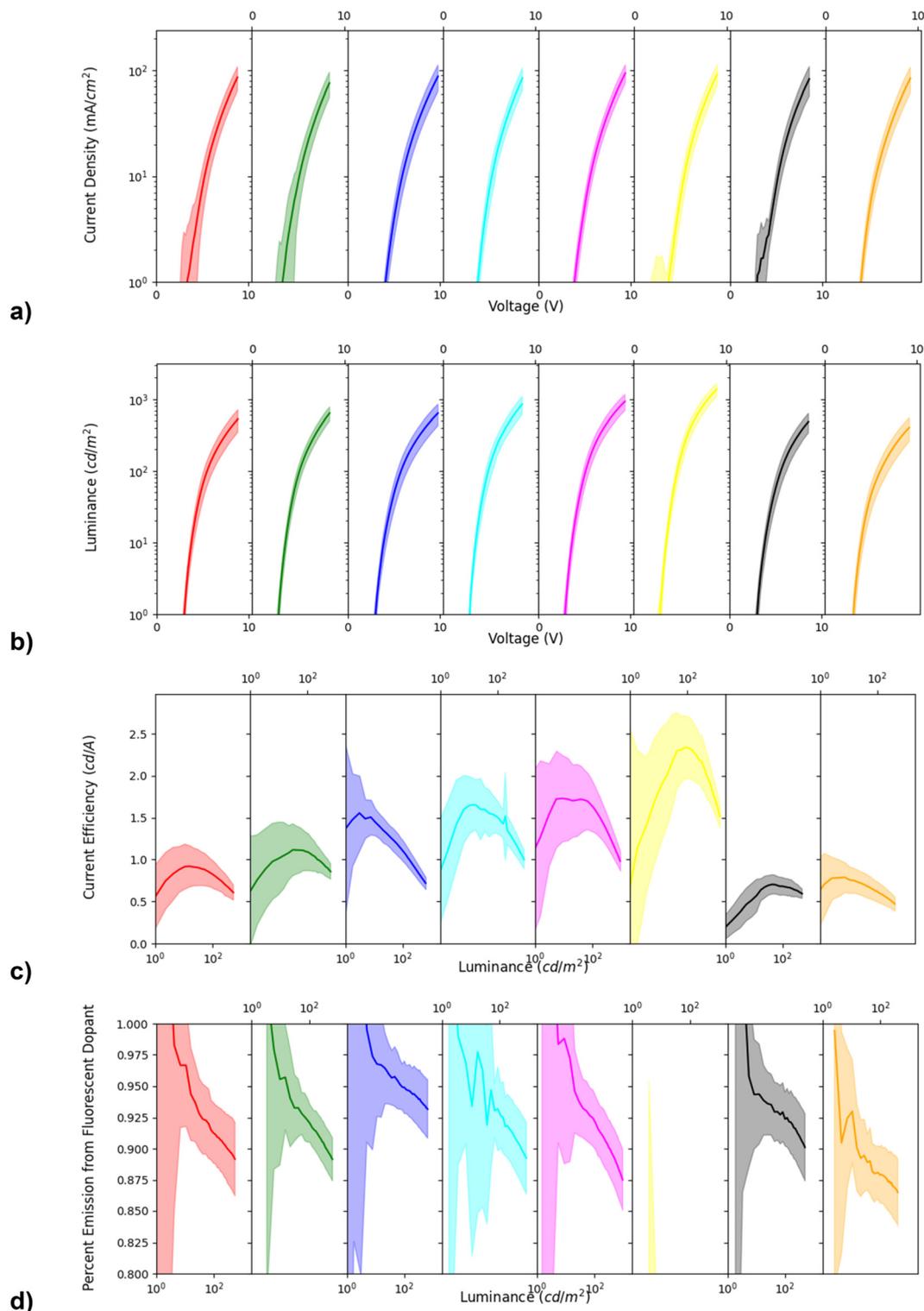

Fig. 6 The emission of TxO-PhCz and the absorption of Cl-BsubPc in toluene.

Fig. 7 Sample spectral output for the FD = BuO-BsubPc (**4**) hyperfluorescent OLEDs, showing the measured emission and the deconvoluted emission; ~525 nm being the emission of the TADF assistant and the ~575 nm being the BuO-BsubPc emission (as an example).
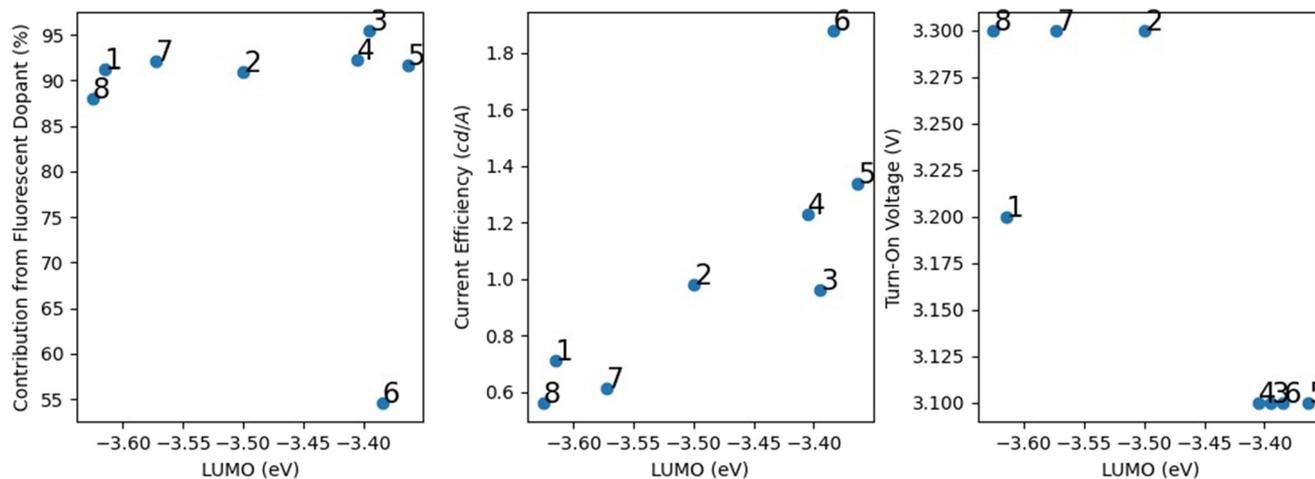
964 | *Mol. Syst. Des. Eng.*, 2025, **10**, 957–969

This journal is © The Royal Society of Chemistry and IChemE 2025

Fig. 8 Average optoelectronic properties for each set of hyperfluorescent OLEDs from material **1** (left) to material **8** (right). The properties shown are (a) current density as a function of applied voltage, (b) measured luminance output as a function of applied voltage, (c) current efficiency as a function of luminance output and the (d) estimated contribution from the fluorescent dopant as a function of luminance output (material **6** was well below the y-axis cutoff of 80% and thus is not shown), estimated by separating the green and orange emission components as illustrated in Fig. 7. The shaded area represents the standard deviation within the set of compositionally variant devices.

only slightly, between 0.1 V and 0.3 V higher than that of the TD-only device. The relative emission contribution from the FD ranged from 88% to 95%, except for the OLEDs using **6**. These devices were brighter due to a significant

This journal is © The Royal Society of Chemistry and IChemE 2025

Mol. Syst. Des. Eng., 2025, **10**, 957–969 | **965**

Fig. 9 Effect of LUMO energy on the turn-on voltage[a], current efficiency[b] and fluorescent dopant contribution[c,d] for hyperfluorescent OLEDs using 20% TXO-PhCz. [a]Turn-on voltage is defined as the voltage that exceeds a luminance of 2 cd m^{-2}. [b]Current efficiency shows the average value above the turn-on voltage, taken as a median across devices in the same set. [c]All values were captured at an output luminance of 250 cd m^{-2}. [d]Defined as the percentage (by intensity) of the FD emission. FD material **1**–**8** BsubPcs (Fig. 1) numbers here.

contribution from the TD that was not transferred to the FD, nearly 50% of the total intensity (Fig. 3, **6b**). An explanation for this inconsistency could be that the long alkyl chains contributed to phase segregation and therefore inefficient transfer in the emissive layer. As shown in Fig. 9, there does appear to be a correlation between the current efficiency and turn-on voltage and the energy levels of the FDs, with BsubPcs with more shallow energy levels demonstrating superior performance. It is possible that this is due to better energetic alignment with the transport layers, as for the baseline devices, leading to improved charge trapping and recombination.[14] Another explanation is that relatively deep LUMO levels of the FD compared to those of the TADF assistant in hyperfluorescent devices can lead to undesirable electron trapping, reducing emission.[18] Overall, the best performing devices in terms of current efficiency, fluorescent dopant contribution and turn-on voltage were those that incorporated the fluorescent dopants **3** and **4**, both with medium-length alkoxy chains as axial groups.

2f. Overall performance. Table 1 shows that the current efficiency of all BsubPc OLEDs increased upon the incorporation of 20% TxOPhCz. This increase ranged between 56% and 318%, with a median of 175% increase (nearly 3-fold). In most cases, the relative contribution from the fluorescent dopant also increased, though in 3 cases (**4**–**6**) it decreased. The best devices, incorporating TxO-PhCz and **4** or **5**, had a current efficiency approaching 2 cd m^{-2}. The three reasons for the success of these hyperfluorescent devices are: i) the good spectral overlap between the TxO-PhCz TADF assistant emission and the absorption spectra of the BsubPcs to facilitate FRET (Fig. 6); ii) the relatively high PLQY of the BsubPcs; iii) the thermal stability of the BsubPcs and TxO-PhCz, facilitating their controlled co-sublimation in a vacuum.

Conclusion

This study reports the best performing OLEDs using BsubPcs as the primary emitters described in the literature, both in terms of current efficiency as a function of luminance and in terms of the relative contribution of the BsubPcs in the emission profile. This increase in performance was due to the incorporation of a TADF assistant molecule, TXO-PhCz, in the demonstration of hyperfluorescence. The choice of the axial group appears to be an important design parameter, potentially through its ability to adjust molecular orbital energetics, with BsubPcs containing butoxy and *tert*-butoxy groups in the boron-bonded axial position demonstrating the best overall performance as fluorescent emitters in hyperfluorescent OLEDs. Further optimization with alternative TADF assistants and BsubPcs with axial or peripheral modifications could lead to an increased understanding of the design space and potentially further improved BsubPc OLED performance. Due to the nuances and complexity of data reporting, especially with large datasets such as that used in this study, we have published the data and processing code online to facilitate future comparisons.

Experimental

Materials

Di-[4-(*N*,*N*-di-*p*-tolyl-amino)-phenyl]cyclohexane (TAPC, sublimed >99.5% purity), 4,4′-bis(carbazol-9-yl)biphenyl (CBP, >99.5% purity), 2-(9-phenyl-9*H*-carbazol-3-yl)-10,10-dioxide-9*H*-thioxanthen-9-one (TXO-PhCz, sublimed >99% purity), 4,6-bis(3,5-di(pyridin-3-yl)phenyl)-2-methylpyrimidine (B3PYMPM, sublimed >99% purity), and 8-hydroxyquinolinolato-lithium (LiQ, sublimed, >99.9%) were obtained from Luminescence Technology Corporation (Lumtec). Aluminum was

966 | *Mol. Syst. Des. Eng.*, 2025, **10**, 957–969

This journal is © The Royal Society of Chemistry and IChemE 2025

obtained from RD Mathis. All BsubPcs were synthesized and purified within our laboratory following published methods;[20] details specific to this work are presented in the ESI.†

OLED fabrication

Glass substrates patterned with indium tin oxide (ITO, Thin Film Devices, Inc.) were manually cleaned using a soap solution (1% Alconox in distilled water) before sonication for 5 minutes each in soapy water, distilled water, acetone and methanol. These substrates were stored in methanol. To prepare an OLED, one substrate was removed from methanol and dried with nitrogen in a laminar flow hood and then treated with oxygen plasma (Harrick Plasma Plasma Cleaner) for 10 minutes. Plasma-treated substrates were transferred into a vacuum chamber that was brought below a pressure of 2×10^{-6} torr. The organics were deposited sequentially through a shadow mask, with a target rate of 1 ± 0.2 Å s^{-1}. For the emissive layer, **1–3** materials (host, TADF assistant (TD), and fluorescent emitter (FD)) were co-deposited at strictly controlled rates totaling 1 Å s^{-1}. Finally, the shadow mask was changed to deposit the LiQ and Al, with target rates of 0.1 Å s^{-1} and 1 Å s^{-1}, respectively. The total area for each OLED formed by the overlap of the ITO and the electrode patterns was 4 mm × 4 mm (16 mm^2). Each substrate contained $n = 20$ OLEDs.

For baseline OLEDs, the device architecture was nominally ITO//dipyrazino[2,3-f:2′,3′-h]quinoxaline-2,3,6,7,10,11-hexacarbonitrile (HAT-CN, 10 nm)//1,1-bis[(di-4-tolylamino)phenyl]cyclohexane (TAPC, 30 nm)//99:1 rate% 4,4′-bis(N-carbazolyl)-1,1′-biphenyl (CBP):FD (20 nm)//4,6-bis(3,5-di(pyridin-3-yl)phenyl)-2-methylpyrimidine (B3PYMPM, 50 nm)//LiF (1 nm)//Al (100 nm). For the hyperfluorescent OLEDs, the emissive layer was replaced with 79:20:1 rate% 4,4′-bis(N-carbazolyl)-1,1′-biphenyl (CBP): 4′-carbazole-9H-thioxanthen-9-one-10,10-dioxide (TXO-PhCz):FD (20 nm).

OLED characterization

OLEDs were characterized in a nitrogen-filled glovebox using a custom-built system. Substrates were fastened into an adjustable holder so that each OLED could be aligned to the entrance to an integrating sphere connected through an optical cable to a high resolution spectrometer (Ocean Insight, HR+D2634). The input voltage and output current were controlled and measured with a Keithley 2614B voltage source. Both Keithley and the spectrometer communicated *via* a USB cable with a LabView program on a desktop computer. OLEDs were characterized from −1 to 12 V with a step of 0.2 V, or until a maximum current of 0.01 A was reached. Spectra at each voltage were recorded over a 50 ms integration time between 380 and 780 nm, at a resolution of 0.5, nm and were calibrated according to the manufacturer's calibration file. All optoelectronic data were processed using the custom Python code, which is available online. Criteria for short-circuited or open-circuit pixels were defined ahead of time as to automatically exclude non-functional pixels from the analysis.

Data availability

Raw data, analytic code, and detailed graphical reporting: **https://github.com/owen-melville/bsubpc-oled-data**.

Author contributions

O. A. M. performed all OLED device fabrication, data acquisition, programming and analysis, writing, and data collation/reporting. R. Z. made all material synthesis, purification, and transferred materials to O. A. M., T. P. performed device design and material thickness measurements and analysis, in consultation with O. A. M. after his graduation from the University of Toronto. This project was completed under the supervision of T. P. B.

Conflicts of interest

The authors declare no competing financial interest.

Acknowledgements

References

1 H. H. P. Gommans, D. Cheyns, T. Aernouts, C. Girotto, J. Poortmans and P. Heremans, Electro-Optical Study of Subphthalocyanine in a Bilayer Organic Solar Cell, *Adv. Funct. Mater.*, 2007, **17**(15), 2653–2658, DOI: **10.1002/adfm.200700398**.

2 R. K. Garner, D. S. Josey, S. R. Nyikos, A. Dovijarski, J. M. Wang, G. J. Evans and T. P. Bender, Boron Subphthalocyanines as Electron Donors in Outdoor Lifetime Monitored Organic Photovoltaic Cells, *Sol. Energy Mater. Sol. Cells*, 2018, **176**, 331–335, DOI: **10.1016/j.solmat.2017.10.018**.

3 A. R. Tetreault, A. Mandlik, K. Wojtkiewicz, K. Nova and T. P. Bender, Outdoor Stability of Triplet Generating and Triplet Harvesting Materials; pentacene and Tetracene Electron Donors Merged with Boron Subphthalocyanines as Electron Acceptors, *ACS Appl. Energy Mater.*, 2023, **6**(5), 3061–3070, DOI: **10.1021/acsaem.2c04185**.

4 W. Chen, B. Han, Q. Hu, M. Gu, Y. Zhu, W. Yang, Y. Zhou, D. Luo, F.-Z. Liu, R. Cheng, R. Zhu, S.-P. Feng, A. B. Djurišić, T. P. Russell and Z. He, Interfacial Stabilization for Inverted Perovskite Solar Cells with Long-Term Stability, *Sci. Bull*, 2021, **66**(10), 991–1002, DOI: **10.1016/j.scib.2021.02.029**.

5 N. Shibata, S. Mori, M. Hayashi, M. Umeda, E. Tokunaga, M. Shiro, H. Sato, T. Hoshi and N. Kobayashi, A phthalocyanine–subphthalocyanine heterodinuclear dimer:

This journal is © The Royal Society of Chemistry and IChemE 2025

Mol. Syst. Des. Eng., 2025, **10**, 957–969 | **967**

comparison of spectroscopic properties with those of homodinuclear dimers of constituting units, *Chem. Commun.*, 2014, **50**(23), 3040–3043, DOI: **10.1039/c3cc49831j**.

6 D. D. Díaz, H. J. Bolink, L. Cappelli, C. G. Claessens, E. Coronado and T. Torres, Subphthalocyanines as Narrow Band Red-Light Emitting Materials, *Tetrahedron Lett.*, 2007, **48**(27), 4657–4660, DOI: **10.1016/j.tetlet.2007.05.036**.

7 G. E. Morse, J. S. Castrucci, M. G. Helander, Z.-H. Lu and T. P. Bender, Phthalimido-Boronsubphthalocyanines: New Derivatives of Boronsubphthalocyanine with Bipolar Electrochemistry and Functionality in OLEDs, *ACS Appl. Mater. Interfaces*, 2011, **3**(9), 3538–3544, DOI: **10.1021/am200758w**.

8 G. E. Morse, M. G. Helander, J. F. Maka, Z.-H. Lu and T. P. Bender, Fluorinated Phenoxy Boron Subphthalocyanines in Organic Light-Emitting Diodes, *ACS Appl. Mater. Interfaces*, 2010, **2**(7), 1934–1944, DOI: **10.1021/am1002603**.

9 M. G. Helander, G. E. Morse, J. Qiu, J. S. Castrucci, T. P. Bender and Z.-H. Lu, pentafluorophenoxy Boron Subphthalocyanine As a Fluorescent Dopant Emitter in Organic Light Emitting Diodes, *ACS Appl. Mater. Interfaces*, 2010, **2**(11), 3147–3152, DOI: **10.1021/am100632y**.

10 T. G. Plint, B. H. Lessard and T. P. Bender, Doping Chloro Boron Subnaphthalocyanines and Chloro Boron Subphthalocyanine in Simple OLED Architectures Yields Warm White Incandescent-like Emissions, *Opt. Mater.*, 2018, **75**, 710–718, DOI: **10.1016/j.optmat.2017.11.028**.

11 N. F. Farac, A. R. Tetreault and T. P. Bender, C₃-Symmetric, Peripherally Fluorinated Boron Subphthalocyanine–Subnaphthalocyanine Hybrids: Shedding New Light on Their Fundamental Photophysical Properties and Their Functionality as Optoelectronic Materials, *J. Phys. Chem. C*, 2023, **127**(1), 702–727, DOI: **10.1021/acs.jpcc.2c07276**.

12 X. Li, S. Fu, Y. Xie and Z. Li, Thermally Activated Delayed Fluorescence Materials for Organic Light-Emitting Diodes, *Rep. Prog. Phys.*, 2023, **86**(9), 096501, DOI: **10.1088/1361-6633/ace06a**.

13 H. Wang, L. Xie, Q. Peng, L. Meng, Y. Wang, Y. Yi and P. Wang, Novel Thermally Activated Delayed Fluorescence Materials–Thioxanthone Derivatives and Their Applications for Highly Efficient OLEDs, *Adv. Mater.*, 2014, **26**(30), 5198–5204, DOI: **10.1002/adma.201401393**.

14 G. Méhes, A. S. D. Sandanayaka, J.-C. Ribierre and K. Goushi, Physics and Design Principles of OLED Devices, in *Handbook of Organic Light-Emitting Diodes*, ed. C. Adachi, R. Hattori, H. Kaji and T. Tsujimura, Springer Japan: Tokyo, 2020, pp. 1–73, DOI: **10.1007/978-4-431-55761-6_49-1**.

15 S. K. Behera and R. D. Costa, Emerging Hyperfluorescent Emitters for Solid-State Lighting, *J. Mater. Chem. C*, 2023, **11**(40), 13647–13656, DOI: **10.1039/D3TC02636A**.

16 H. Nakanotani, T. Higuchi, T. Furukawa, K. Masui, K. Morimoto, M. Numata, H. Tanaka, Y. Sagara, T. Yasuda and C. Adachi, High-Efficiency Organic Light-Emitting Diodes with Fluorescent Emitters, *Nat. Commun.*, 2014, **5**(1), 4016, DOI: **10.1038/ncomms5016**.

17 N. R. Wallwork, M. Mamada, A. Shukla, S. K. M. McGregor, C. Adachi, E. B. Namdas and S.-C. Lo, High-Performance Solution-Processed Red Hyperfluorescent OLEDs Based on

Cibalackrot, *J. Mater. Chem. C*, 2022, **10**(12), 4767–4774, DOI: **10.1039/D1TC04937B**.

18 Y. H. Jung, D. Karthik, H. Lee, J. H. Maeng, K. J. Yang, S. Hwang and J. H. Kwon, A New BODIPY Material for Pure Color and Long Lifetime Red Hyperfluorescence Organic Light-Emitting Diode, *ACS Appl. Mater. Interfaces*, 2021, **13**(15), 17882–17891, DOI: **10.1021/acsami.1c03175**.

19 D. J. Shin, S. J. Hwang, J. Lim, C. Y. Jeon, J. Y. Lee and J. H. Kwon, Reverse Intersystem Crossing Accelerating Assistant Dopant for High Efficiency and Long Lifetime in Red Hyperfluorescence Organic Light-Emitting Diodes, *Chem. Eng. J.*, 2022, **446**, 137181, DOI: **10.1016/j.cej.2022.137181**.

20 R. Zigelstein and T. P. Bender, Boron Subphthalocyanine Axial Groups: A Comprehensive Set for Studying the Tuning of Photophysical and Electrochemical Properties, *Mol. Syst. Des. Eng.*, 2024, **9**, 856–874, DOI: **10.1039/D4ME00070F**.

21 K. L. Sampson, X. Jiang, E. Bukuroshi, A. Dovijarski, H. Raboui, T. P. Bender and K. M. Kadish, A Comprehensive Scope of Peripheral and Axial Substituent Effect on the Spectroelectrochemistry of Boron Subphthalocyanines, *J. Phys. Chem. A*, 2018, **122**(18), 4414–4424, DOI: **10.1021/acs.jpca.8b02023**.

22 E. Bukuroshi, A. U. Petersen, L. Brøløs, T. P. Bender and M. B. Nielsen, Exploring the Synthesis and Electronic Properties of Axially Substituted Boron Subphthalocyanines with Carbon-Based Functional Groups, *Eur. J. Inorg. Chem.*, 2020, **2020**(36), 3481–3495, DOI: **10.1002/ejic.202000525**.

23 G. Li and S. Zheng, A Computational Study of the Effects of Axial Halogen Substitutions of Boron Subphthalocyanines on Their Electronic Spectra in Solution and in the Solid State, *Spectrochim. Acta, Part A*, 2019, **222**, 117180, DOI: **10.1016/j.saa.2019.117180**.

24 M. Hildebrand, D. Holst, T. Bender and L. Kronik, Electronic Structure, Bonding, and Stability of Boron Subphthalocyanine Halides and Pseudohalides, *Adv. Theory Simul.*, 2022, **5**(4), 2100400, DOI: **10.1002/adts.202100400**.

25 S. Negi, P. Mittal and B. Kumar, Impact of Different Layers on Performance of OLED, *Microsyst. Technol.*, 2018, **24**(12), 4981–4989, DOI: **10.1007/s00542-018-3918-y**.

26 W. H. Lee, D. H. Kim, P. J. Jesuraj, H. Hafeez, J. C. Lee, D. K. Choi, T.-S. Bae, S. M. Yu, M. Song, C. S. Kim and S. Y. Ryu, Improvement of Charge Balance, Recombination Zone Confinement, and Low Efficiency Roll-off in Green Phosphorescent OLEDs by Altering Electron Transport Layer Thickness, *Mater. Res. Express*, 2018, **5**(7), 076201, DOI: **10.1088/2053-1591/aacec6**.

27 N. C. Erickson and R. J. Holmes, Investigating the Role of Emissive Layer Architecture on the Exciton Recombination Zone in Organic Light-Emitting Devices, *Adv. Funct. Mater.*, 2013, **23**(41), 5190–5198, DOI: **10.1002/adfm.201300101**.

28 J. W. Park, D. C. Shin and S. H. Park, Large-Area OLED Lightings and Their Applications, *Semicond. Sci. Technol.*, 2011, **26**(3), 034002, DOI: **10.1088/0268-1242/26/3/034002**.

29 H. Li, R. Komatsu, J. Hankache, H. Sasabe, L. M. Lawson Daku, B. Özen, S. Chen, J. Hauser, A. Hauser, S. Decurtins, J. Kido and S.-X. Liu, Bis(Triphenylamine)Benzodifuran

968 | *Mol. Syst. Des. Eng.*, 2025, **10**, 957–969

This journal is © The Royal Society of Chemistry and IChemE 2025

Chromophores: Synthesis, Electronic Properties and Application in Organic Light-Emitting Diodes, *Front. Chem.*, 2021, **9**, 721272, DOI: **10.3389/fchem.2021.721272**.

30 Y.-S. Park, W.-I. Jeong and J.-J. Kim, Energy Transfer from Exciplexes to Dopants and Its Effect on Efficiency of Organic Light-Emitting Diodes, *J. Appl. Phys.*, 2011, **110**(12), 124519, DOI: **10.1063/1.3672836**.

31 C. Murawski, K. Leo and M. C. Gather, Efficiency roll-off in organic light-emitting diodes, *Adv. Mater.*, 2013, **25**(47), 6801–6827, DOI: **10.1002/adma.201301603**.

This journal is © The Royal Society of Chemistry and IChemE 2025

Mol. Syst. Des. Eng., 2025, **10**, 957–969 | **969**